Diffusion Coefficients in the Lateral Intercellular Spaces of Madin-Darby Canine Kidney Cell Epithelium Determined with Caged Compounds

Ping Xia,* Peter M. Bungay,# Carter C. Gibson,* Olga N. Kovbasnjuk,* and Kenneth R. Spring*
*Laboratory of Kidney and Electrolyte Metabolism, National Heart, Lung and Blood Institute, and #Biomedical Engineering and Instrumentation Program, National Center for Research Resources, National Institutes of Health, Bethesda, Maryland 20892

ABSTRACT The diffusion coefficients of two caged fluorescent dyes were measured in free solution and in the lateral intercellular spaces (LIS) of cultured Madin-Darby canine kidney (MDCK) cells after photoactivation by illumination with a continuous or pulsed UV laser. Both quantitative video imaging and a new photometric method were utilized to determine the rates of diffusion of the caged fluorescent dyes: 8-((4,5-dimethoxy-2-nitrobenzyl)oxy)pyrene-1,3,6-trisulfonic acid (DMNB-HPTS) and (4,5-dimethoxy-2-nitrobenzyl) fluorescein dextran (10,000 MW) (DMNB-caged fluorescein dextran). The diffusion coefficients at 37°C in free solution were 3.3×10^{-6} cm^2/s (HPTS) and 0.98×10^{-6} cm^2/s (10,000 MW dextran). Diffusion of HPTS within nominally linear stretches of the LIS of MDCK cells grown on glass coverslips was indistinguishable from that in free solution, whereas dextran showed a 1.6 ± 0.5-fold reduction in diffusivity. Measurements of HPTS diffusion within the LIS of multicellular regions also exhibited a diffusivity comparable to the free solution value. The restriction to diffusion of the dextran within the LIS may be due to molecular hindrance.

INTRODUCTION

Solute diffusion coefficients figure prominently in estimating the thickness of unstirred fluid layers on the apical or basolateral surfaces of epithelia and in characterizing the properties of interstitial spaces. The diffusion coefficient for small solutes in the lateral intercellular spaces (LIS) of transporting epithelia also plays a crucial role in most models of fluid transport (Diamond, 1979). The determination of solute diffusion coefficients within the interstitial spaces of epithelial tissues has been difficult because of technical limitations posed by the small distances that reduce the time available for measurement and by the complex interstitial geometry. In addition, local diffusion coefficients may differ from the average values determined over larger areas.

Measurements of the diffusion coefficients of fluorescently labeled compounds of biological import within biologically relevant compartments, such as cell membranes, have generally utilized fluorescence recovery after photobleaching (FRAP) (Axelrod et al., 1976; Edidin et al., 1976). In epithelia, FRAP has also been used to determine the diffusion coefficient of the dye BCECF (2′,7′-bis(carboxyethyl)-5,6-carboxyfluorescein) in the lateral intercellular spaces (LIS) of Madin-Darby canine kidney (MDCK) cells grown on glass coverslips (Harris et al., 1994), the flow rate of perfusate in the lumen of isolated renal tubules (Flamion et al., 1991), and the rate of diffusion of Na^+ channels within the membrane of cultured renal A6 cells (Smith et al., 1995). FRAP may suffer from significant signal-to-noise and dynamic range limitations, as the intensity of a dim region must be measured in the presence of a bright background (Adams and Tsien, 1993).

To overcome some of the limitations of the previous approaches, we utilized photoactivatable or "caged" fluorophores, employed an uncaging beam optical geometry that simplified the analysis, and developed new high-speed, multichannel, photomultiplier detector instrumentation for the determination of the diffusion coefficients of solutes of both low and high molecular weights. Caged fluorophores are virtually nonfluorescent until activated by short wavelength illumination. This technique, called photoactivated fluorescence (PAF), has been utilized to track motion within cells (Mitchison, 1989; Svoboda et al., 1996), as well as convective flow (Lempert et al., 1995). The geometry of the pulsed laser illumination system was chosen to result in an uncaging beam of uniform diameter through the entire thickness of the MDCK cell layer. Thus axial spread of uncaged fluorophore was eliminated, and the analysis was simplified to one-dimensional diffusion. The combination of high-speed photodetection and video imaging resulted in a powerful method for the selection of the site of uncaging and accurate recording of the spread of uncaged fluorophore with high temporal resolution. Using PAF, we measured the diffusion coefficients of a fluorescently labeled dextran of 10,000 MW and the small pH-sensitive solute HPTS (8-hydroxypyrene-1,3,6-trisulfonic acid, MW 524) in free solution and within the LIS of MDCK cells grown on glass coverslips.

Received for publication 3 November 1997 and in final form 2 March 1998.

Address reprint requests to Dr. Kenneth R. Spring, National Institutes of Health, Building 10, Room 6N260, 10 Center Dr., MSC 1603, Bethesda, MD 20892-1603. Tel.: 301-496-3236; Fax: 301-402-1443; E-mail: springk@fido.nhlbi.nih.gov.

0006-3495/98/06/3302/11 $2.00

MATERIALS AND METHODS

Cell culture

Low-resistance MDCK cells (passage 64–76 from the American Type Culture Collection, Rockville, MD) were cultured as previously described (Harris et al., 1994), using Dulbecco's modified Eagle medium (DMEM) and 2 mM glutamine without riboflavin, antibiotics, or phenol red. The

culture medium for stock cells was supplemented with 10% fetal bovine serum (Gibco, Grand Island, NY). The cells were grown to confluence on 25-mm coverslips in DMEM supplemented with 5% fetal bovine serum for 5–12 days. The Ringer's perfusion solution contained (mM): 142 Na^+, 5.3 K^+, 1.8 Ca^{2+}, 0.8 Mg^{2+}, 127 Cl^-, 24 HCO_3^-, 5.6 glucose. The solution was equilibrated in the perfusion bottles with 97% air/3% CO_2 at 39°C to give pH 7.4 at 37°C in the perfusion chamber. The HEPES-buffered Ringer's was similar in composition, except that it was free of HCO_3^-, contained 14 mM HEPES and 137 mM Cl^-, and was bubbled with room air.

Chemicals

The caged fluorescent dyes were obtained from Molecular Probes (Eugene, OR): 8-((4,5-dimethoxy-2-nitrobenzyl)oxy)pyrene-1,3,6-trisulfonic acid, trisodium salt (DMNB-caged HPTS); and (4,5-dimethoxy-2-nitrobenzyl)fluorescein dextran (MW 10,000).

Fluorescence microscopy

The experiments were performed on the stage of an inverted microscope (Diaphot; Nikon, Melville, NY) modified for simultaneous transmitted light differential interference contrast (DIC) and low light level fluorescence (Spring, 1990). A block diagram of the system is shown in Fig. 1. The monolayers were observed with a 100×/1.3 N.A. objective lens (Nikon). For fluorescence excitation during the uncaging and subsequent measurement periods, the cells were epiilluminated with a 24-μm-radius spot of laser light at 458 or 488 nm (532 Argon laser; Omnichrome, Chino, CA) at an incident light flux of ~40 $\mu W/cm^2$ (measured at the back focal plane of the objective lens). The multiline laser output passed through an AOTF (acoustooptical tunable filter) (TEAF-40.55; Brimrose Corp., Baltimore, MD) that allowed rapid (~1 ms) wavelength and power switching. The microscope output port was connected to a Multi-image Module (Nikon) in which the light was either divided equally between an intensified CCD camera (ICCD) and a multichannel photomultiplier tube (PMT) or sent exclusively to the ICCD. The ICCD consisted of an image intensifier (KS-1381; Video Scope International, Sterling, VA) optically coupled to a CCD camera (CCD-72; Dage-MTI, Michigan City, IN). Images were stored on an OMDR (optical memory disk recorder) (TQ2028-F; Panasonic, Secaucus, NJ) for subsequent off-line analysis. The multichannel PMT is described below, in detail. The sequence of events (e.g., solution valves, video gain, illumination intensity, focus position) during the experiment was controlled by a computer using customized software.

Multichannel PMT

A multianode detector arranged as an 8 × 8 array of photomultiplier tubes in a 20-mm-square pattern has recently become commercially available (XP1722/A; Philips Photonics, Slatersville, RI). Each PMT is 2.54 mm square, with a nominal gain of 1.1×10^6 and a total dark current of <1 nA. The bialkali photocathode is covered by a fiber-optic window and exhibits a peak sensitivity of 61 mA/W at 407 nm. High voltage was supplied by a remotely controlled supply (SHV12–1.0K2000; Spellman High Voltage Electronics Corp., Plainview, NY). The detector was connected through a voltage divider network (VD107; Philips) and a zero insertion force socket (FE4164; Philips) to a customized assembly consisting of four 16-channel drift chamber amplifier-discriminators (2735DC/MOD100; LeCroy Corp., Chestnut Ridge, NY) connected in parallel. The outputs of the amplifier-discriminators were coupled to two 32-channel latching scalers (4434; LeCroy) mounted in a CAMAC minicrate (465; Jorway Corp., Westbury, NY). The output of the CAMAC crate was connected by a SCSI bus to a Pentium computer.

All 64 channels, operating in the photon-counting mode, achieved a maximum sampling rate of 1 kHz with a dark count of 0.05–0.1 counts/sample. The maximum count within the linear range of operation was ~300,000/sample. Gain was determined independently for each channel, and a table of gain correction values was generated. Customized software was developed that permitted acquisition of data before and after an uncaging pulse and subsequent plotting of selected channels.

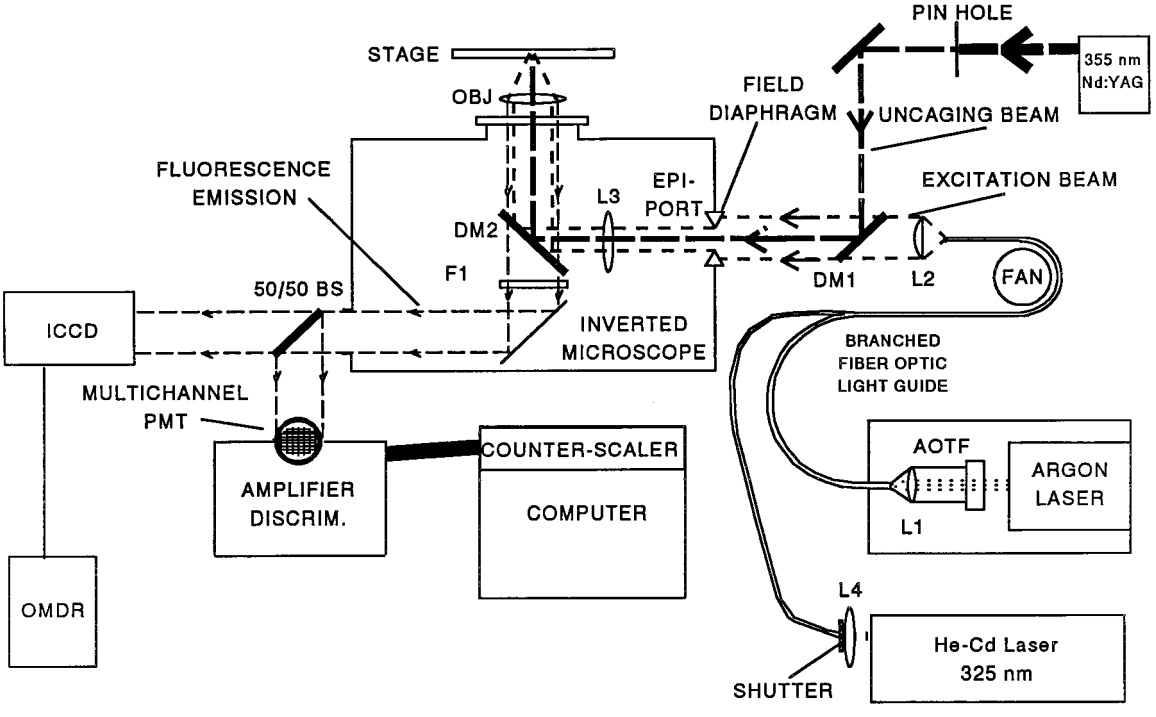

FIGURE 1 System diagram. DM, Dichromatic mirror; L, lens; F, filter; BS, beam splitter, OBJ, objective lens; AOTF, acoustooptic tunable filter; ICCD, intensified CCD camera; OMDR, optical memory disk recorder. See text for details.

Uncaging illumination system

Two laser light sources were employed for photoactivation of caged dyes: 1) a He-Cd laser emitting continuously at 325 nm with an output power of 21 mW (3056–15; Omnichrome); and 2) a frequency-tripled Nd:YAG laser (Minilite-10; Continuum, Santa Clara, CA) that produced a maximum output of ~4 mJ at 355 nm with a pulse duration of 4–6 ns, and a repetition rate of 10 Hz. Fig. 1 shows that the output of the He-Cd laser was coupled to the microscope epiillumination port through a branched optical fiber, as described previously (Xia et al., 1995). The He-Cd output intensity was used for experiments involving uncaging of larger areas (24 μm radius) comparable to the field of view of the intensified CCD camera.

The Nd:YAG laser output was utilized for spot irradiation of a small, well-defined region to achieve virtually instantaneous release of caged fluorophores. The output of the laser was passed through a 1-mm-diameter pinhole to ensure Gaussian beam geometry, and then reflected by a dichromatic mirror (DM1 in Fig. 1) into the center of the field of view. The beam was not expanded or focused before the microscope objective lens, and thus remained as a low-aperture beam (approximate NA = 0.2) with a diameter of ~3 μm in the image plane. As determined from studies on fluorescently stained films of known thickness, the uncaging beam diameter remained at ~3 μm for at least 5 μm above and below the focal plane. The full output power of the Nd:YAG laser was significantly greater than required for uncaging and caused substantial photodynamic damage to the preparation and to the microscope optics. The laser was therefore operated in the low-power mode with a beam energy of ~0.5 mJ/pulse.

Spectral scanning

Excitation and emission spectra of all dyes used in the study were obtained in HEPES-buffered Ringer's solution in a spectrofluorimeter (FluoroMax; Spex Industries, Edison, NJ) as previously described (Xia et al., 1995).

Perfusion chamber

The coverslips with adherent cells were loaded into an open perfusion chamber, as described previously (Xia et al., 1995). Perfusion rates were adjusted to ~10–12 μl/min. The volume of the bath in the perfusion chamber was ~10 μl. The perfusion chamber was maintained at 37°C, and the rate of perfusion was controlled by hydrostatic pressure as previously described (Harris et al., 1994).

Dye loading into the LIS

Dyes were microinjected into fluid-filled domes of confluent MDCK monolayers, as previously described (Xia et al., 1995). In brief, the tip of a sharpened, 5-μm-diameter glass micropipette was filled with an 0.5 mM solution of the fluorescent dye in HEPES-buffered Ringer's solution. A dome was punctured, and ~10 pl of the dye was microinjected using gas pressure (5242; Eppendorf, Madison, WI). The area selected for imaging was at least three cells away from the dome.

Statistics

Data are presented as means ± SD. Statistical significance was determined using the paired or unpaired *t*-test, and a *p* value less than 0.05 was considered significant.

Theory and analysis of fluorescence microscopy images

Four experimentally relevant situations are considered. In all cases except the last (uncaging of diffusible dye within the LIS of many cells in a monolayer), the uncaging beam was assumed to be of uniform and constant diameter through the entire axial distance of interest.

Determination of the uncaging rate constant by uncaging of dye immobilized in a thin viscous film

The caged compound is initially present at uniform concentration, C_c^0. The viscosity of the glycerin solution is assumed to be sufficiently high that diffusion can be neglected. Ultraviolet illumination is supplied at time $t = 0$. In keeping with the uncaging beam geometry, the local light intensity, I_u, is assumed to be uniform in the transverse direction, but may vary radially relative to the beam axis. The rate of disappearance of the caged reactant is assumed to be proportional to the concentration of the caged compound, C_c, with a rate constant, k, for the reaction that is proportional to the intensity of the uncaging beam,

$$k[\rho] = \alpha_u I_u[\rho], \tag{1}$$

where α_u is a proportionality constant. The bracketed expressions indicate that the intensity and, hence, the rate constant may vary with radial position ρ. The appearance of the uncaged dye is thus given by

$$C_u[\rho, T_u] = C_c^0(1 - e^{-k[\rho]T_u}), \tag{2}$$

where T_u is the duration of the uncaging time interval. At the end of this interval, $t = T_u$, the UV uncaging light is instantaneously extinguished, and fluorescence, stimulated by 458-nm or 488-nm wavelength excitation of uniform intensity over a 24-μm-radius spot, is monitored at the appropriate emission wavelength. The emitted light intensity from the uncaged product is assumed to vary in proportion to the local uncaged concentration. Within a cylindrical region of radius ρ_s, equal to or smaller than the radius of the illumination beam, the fluorescence can be represented by

$$F[T_u] = F^* + 2\pi\alpha_i\phi\int_0^{\rho_s} C_u[\rho, T_u]\rho\, d\rho, \tag{3}$$

in which F^* is the background fluorescence, α_i is a proportionality coefficient of conversion from concentration to light intensity, and $\phi = 1$ is the volume fraction of the film occupied by solution. Substituting Eq. 2 into Eq. 3 leads to

$$F[T_u] = F^* + \pi\alpha_i\phi C_c^0\left(\rho_s^2 - 2\int_0^{\rho_s} e^{-k[\rho]T_u}\rho\, d\rho\right). \tag{4}$$

For large values of $t = T_u$, provided that $k[\rho] \neq 0$ for $0 \leq \rho \leq \rho_s$, Eq. 4 becomes

$$F^\infty = F^* + \pi\rho_s^2\,\alpha_i\phi C_c^0. \tag{5}$$

Hence Eq. 4 can be rewritten in normalized form as

$$\frac{F^\infty - F[T_u]}{F^\infty - F^*} = \left(\frac{2}{\rho_s^2}\right)\int_0^{\rho_s} e^{-k[\rho]T_u}\rho\, d\rho. \tag{6}$$

Two uncaging beams were utilized. These were of different nominal radius, ρ_u, and different profiles: a small spot with a Gaussian profile and a large circular area with a "top hat" profile. For a Gaussian beam profile, Eq. 1 was then replaced by the empirical expression

$$k[\rho] = Ke^{-(\rho/\rho_u)^2}, \tag{7}$$

With a large-diameter uncaging beam, an empirical expression, derived from the measured beam profile in Fig. 2 *a*, was used:

$$k[\rho] = \frac{1}{2} K\left(1 - \tanh\left[\frac{(\rho/\rho_u) - 1}{\sigma_h}\right]\right), \quad (8)$$

in which σ_h is the constant for the top hat beam. The shape of the normalized approximation function $k[\rho]/K$ in Eq. 8 is shown in Fig. 2 *b* for $\sigma_h = 0.3$. As $\sigma_h \to 0$, the value of the normalized function approaches unity for all ρ in the interval $0 \le \rho < \rho_u$, and Eq. 6 simplifies to

$$\ln\left(\frac{F^\infty - F[T_u]}{F^\infty - F^*}\right) = -KT_u. \quad (9)$$

Uncaging of diffusible dye in a thin film

In this situation both the caged and uncaged species are allowed to diffuse freely. The concentrations are assumed to be uniform in the transverse direction, because a relatively small fraction of the incident light is absorbed. Diffusion will then lie in the plane of the film, and the fluorescence from a region bounded by $\rho = \rho_s$ at any time t is given by the following variation of Eq. 3:

$$F = F^* + 2\pi\alpha_i\phi \int_0^{\rho_s} C_u[\rho, t]\rho \, d\rho. \quad (10)$$

To avoid the need to determine values for the constants α_i and ϕ, the fluorescence values can be normalized relative to the fluorescence, F^{ref}, at a particular arbitrary reference time, t^{ref}, in a manner analogous to that of Eq. 6:

$$\frac{F - F^*}{F^{ref} - F^*} = \frac{\int_0^{\rho_s} C_u[\rho, t]\rho \, d\rho}{\int_0^{\rho_s} C_u[\rho, t^{ref}]\rho \, d\rho}. \quad (11)$$

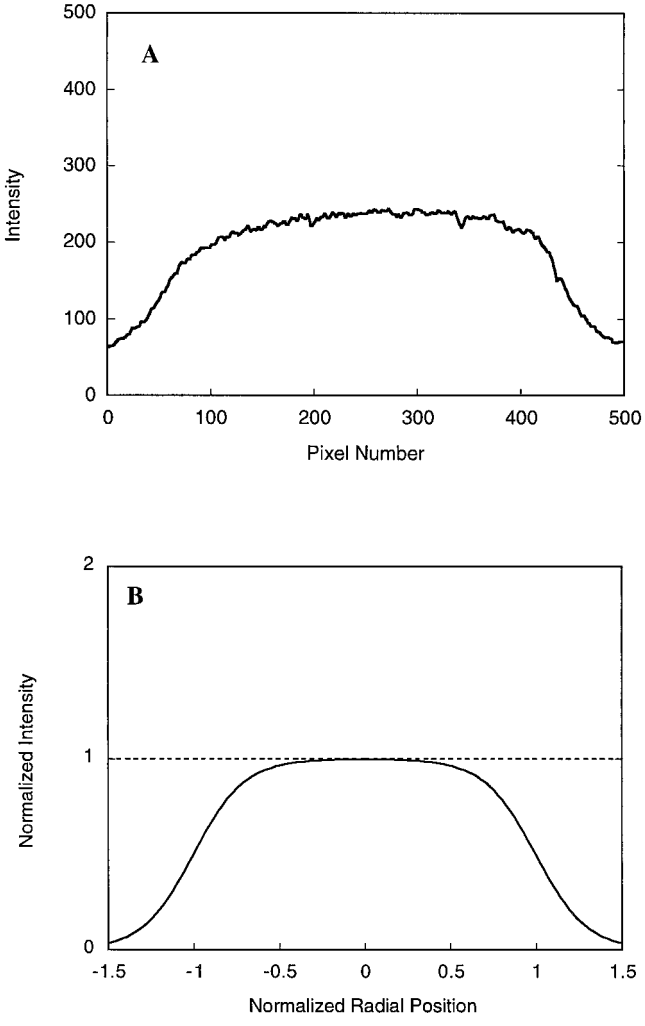

FIGURE 2 (*a*) Measured spatial profile of the top hat uncaging beam intensity. (*b*) Normalized function, k/K, from Eq. 8, used to approximate the radial variation in intensity of illumination beam for $\sigma_h = 0.3$. The radial position is normalized with respect to the nominal beam radius.

Rapid uncaging within a small region of LIS

The cross section of the Gaussian uncaging beam was small compared with a single epithelial cell. Consequently, the uncaging could be confined to nominally straight and narrow segments of LIS, or alternatively, the spot could be positioned over the junction of three or more cells such that multiple narrow LIS segments radiate from the spot center. For such situations, it is assumed that the diffusion can be treated as rectilinear, instead of radial. Solute diffusion, however, may also be slowed as a result of hindrance effects within the LIS. The reduction in diffusivity will be ascribed to a hindrance factor, θ, defined by

$$\theta = \frac{D_{free}}{D_{LIS}}, \quad (12)$$

in which D_{LIS} is the measured diffusion coefficient within the LIS and D_{free} is the free solution value.

The small spot size permits the use of high-intensity, short-duration uncaging pulses. For sufficiently short pulses, diffusion of both the caged and uncaged species can be neglected in the ~5-ns uncaging interval. Under these conditions, the only diffusion to be considered in the postuncaging period is that of the uncaged dye. For rectilinear diffusion in the direction of the coordinate x,

$$C_u[x, 0] = C_u^0 e^{-(x/x_u)^2}, \quad (13)$$

in which x_u, the nominal half-length of the Gaussian uncaging beam, is equal in magnitude to the nominal beam radius ρ_u. This uncaged dye concentration profile is an approximation consistent with the empirical Gaussian spatial profile of the uncaging rate constant in Eq. 7. Assuming that all of the solute remains within the LIS during the postuncaging interval leads to the conservation constraint

$$\int_0^\infty C_u[x, t] \cdot dx = C_u^0 x_u \frac{\sqrt{\pi}}{2}, \qquad \text{for all } t \ge 0. \quad (14)$$

Uncaging of diffusible dye within the LIS of many cells in a monolayer

When the radius of the circular uncaging region is large compared with the dimensions of an individual epithelial cell, the LIS geometry is too complex to be specified directly, even though the effect of LIS variation in the transverse direction is assumed to be negligible. To simplify the analysis, the complex two-dimensional problem of diffusion within the LIS is replaced by a one-dimensional problem of radial diffusion. This is effected by introducing a cellular-scale geometric tortuosity factor, Λ^2, that accounts for the nonradial orientation of the various LIS segments. The effective radial diffusion coefficients for either the caged or uncaged

species will then be represented by

$$D_{EFF} = \frac{D_{LIS}}{\Lambda^2}, \tag{15}$$

The geometric tortuosity factor, Λ, represents the increase in the LIS diffusional path length relative to that for unidirectional diffusion along a straight LIS segment. For a repetitive unit cell whose characteristic dimension in the plane of the monolayer is small compared with the radius of the uncaging beam, the geometric tortuosity factor can be approximated by

$$\Lambda = \frac{p}{2d}, \tag{16}$$

where p is the perimeter and d is the equivalent diameter, given by

$$d \equiv \sqrt{\frac{4A}{\pi}}, \tag{17}$$

where A is the smooth surface area of the apical membrane. The measured means ± SD for an MDCK cell in monolayers are $p = 29.1 \pm 1.5$ μm, $A = 53.5 \pm 4.2$ μm^2, $d = 8.25$ μm, and, from Eq. 16, $\Lambda^2 = 3.1$.

Data analysis

Determination of the rate of uncaging of immobilized dye

The rate constant for uncaging of C-HPTS in a thin film of 97% glycerin, K, was evaluated by nonlinear regression of Eq. 9 to the fluorescence data. The regression employed a modified Marquardt-Levenberg subroutine (DUNLSJ; IMSL, Houston, TX). The values of the background fluorescence, F^*, and the fluorescence for complete uncaging, F^∞, were determined as fitting parameters, along with K.

Uncaging of diffusible dye in a thin film

The diffusion coefficients of HPTS and 10,000 MW dextran were evaluated by Marquardt-Levenberg nonlinear regression of Eq. 11 to the PMT readings obtained after uncaging. The fluorescence from the thin film was collected from a single PMT (12.6 μm × 12.6 μm effective size in the image plane) encompassing the 3-μm-diameter spot in which uncaging occurred. The PMT readings were recorded at 5- or 10-ms intervals for periods 1.5–15 s in duration. Both the original data and records smoothed by averaging successive equal-numbered groups of 2 to 5 readings were analyzed. The reference time in Eq. 11 was chosen to be the instant after the uncaging pulse. A simplifying assumption was that no dye diffusion occurs during the 4–6-ns uncaging pulse interval.

The dye concentration profile, $C_u[\rho, t]$, was generated by solution of the partial differential mass balance equations. The numerical solution utilized the method of lines subroutine (DMOLCH; IMSL). Instead of performing the integration in Eq. (11) over a square area of dimension 12.6 μm × 12.6 μm, the radius, ρ_s, was set equal at 7.1 μm, the value for a circular region of equivalent area. The initial postuncaging PMT reading (F^{ref}) and the diffusion coefficient, D_{free}, were two adjustable parameters whose values were simultaneously estimated by Marquardt-Levenberg regression. The recording duration was generally sufficient to obtain the background level (F^*) from the final readings of each run.

Rapid uncaging within a small region of LIS

Values for the diffusion coefficient of HPTS and the 10,000 MW dextran within the LIS were obtained by two approaches, both of which used the method of lines (DMOLCH) numerical solution to the mass balance equations to fit to the fluorescence measurements. One approach fit the numerical simulations to the measured time decay of uncaged fluorescence intensity, I[t], at a location, $x = 0$, near the center of the uncaging spot. For the video images, the earliest reliable intensity values were recorded at least 0.2 s after the end of the uncaging pulse. Consequently, for nonlinear Marquardt-Levenberg regressions to the time decay data, it was necessary to include the initial postuncaging fluorescence, $I[T_u]$ at $x = 0$, as well as the diffusion coefficient, D_μ, as adjustable parameters. The covariance between the two parameters in the video images was too large to yield reliable estimates by this method. Therefore, this approach was not used for the analysis of data derived from video images, but it worked very well with the measurements obtained from the multichannel PMT.

In the second approach, the numerical solution was fit to the spatial fluorescence intensity profile along the LIS, $I[x, t_1]$, obtained from the video image at an early postuncaging time point, $t = t_1$, usually 0.2 s. Nonlinear Marquardt-Levenberg regressions to the spatial intensity profiles were performed with D_μ as the only adjustable parameter by invoking the assumption that the amount of uncaged dye within the LIS remains constant over the postuncaging period. This constraint, expressed in Eq. 14, leads to a corresponding conservation of fluorescence condition,

$$F[t] = F^* + \alpha_i \phi x_u C_u^0 \frac{\sqrt{\pi}}{2} = \text{constant}, \tag{18}$$

in which $x_u = 1.5$ μm is the half-width of the uncaging region for a 3-μm-diameter spot.

Uncaging over a monolayer region containing many cells

For the large-diameter top hat uncaging beam, the relatively low excitation intensity necessitated uncaging intervals of 3 s duration. It was necessary to include both diffusion and the interconversion reaction kinetics during the uncaging interval. Unsteady partial differential mass balance equations were formulated that describe diffusion with first-order reactions for the caged and uncaged species. These balance equations utilize diffusion coefficients as defined in Eq. 15 for the two species and the uncaging rate constant defined in Eq. 8. The value for K was used in the analysis of video images of the uncaging and diffusion of HPTS in MDCK monolayers. The hindrance factor, θ, from Eq. 12 was determined by Marquardt-Levenberg regression in which the time decay in the fluorescence predicted from the numerical solution was fit to the measured LIS fluorescence within the monitoring region of the same radius as the uncaging beam, 24 μm. The measured fluorescence was normalized according to Eq. 11. The first measurement obtained after the end of the uncaging interval was chosen as the reference fluorescence value, F^{ref}. The background fluorescence, F^*, was treated as an adjustable parameter and was evaluated simultaneously with θ.

RESULTS

Uncaging HPTS in a cuvette

Uncaging of the DMNB group is generally achieved with UV irradiation at wavelengths between 350 and 400 nm (Adams and Tsien, 1993; Kaplan et al., 1978). The photon flux required for uncaging HPTS was experimentally determined, because the HPTS moiety shows significant absorbance between 330 and 380 nm (Wolfbeis et al., 1983), a factor that is expected to reduce the efficiency of uncaging. The uncaging efficiency was evaluated at three wavelengths between 325 nm and 350 nm (Table 1). Solutions of caged HPTS, in a quartz cuvette, were irradiated repetitively for a measured time period with a measured UV photon flux, and the extent of uncaging was determined from the resultant fluorescence emission at 520 nm. Fluorescence was measured after each irradiation period by inserting the cuvette into a spectrofluorimeter. The extent of uncaging was plot-

TABLE 1 Uncaging HPTS

Wavelength (nm)	Intensity (photons/s-cm^2)	Time constant (s)	Uncaging rate (molecules/s)	Effective quantum yield (photons/molecule)
325	3.7×10^{16}	355	2.7×10^9	409
340	1.4×10^{16}	705	1.4×10^9	410
350	1.4×10^{16}	480	2.0×10^9	305

A 0.25-ml volume of a 17.5 nM solution of HPTS was placed in a quartz cuvette and exposed to the UV beam for 60 s. The UV beam was collimated to uniformly illuminate the 0.25 cm^2 area of solution, and the fluorescence of the uncaged species was measured in a spectrofluorimeter as described in the Methods. Exposure to the UV beam was repeated until all uncaging was complete, as indicated by no additional increase in fluorescence. The time constant for uncaging was determined by the method of least squares from the measured HPTS fluorescence. An extinction coefficient of 4500 M^{-1} cm^{-1} was assumed for caged HPTS in calculation of the effective quantum yield.

ted as a function of the incident UV photon flux, and a curve was fitted to the data by the method of least squares.

Table 1 shows the results of these determinations, assuming an extinction coefficient for caged HPTS of 4500 M^{-1} cm^{-1}. The rate of uncaging was first order and was not sensitive to variations in the wavelength of UV irradiation over the range 325–366 nm. Between 300 and 400 photons were required to uncage each molecule of HPTS, resulting in an apparently low efficiency for uncaging of ~0.33%. A quantum yield of 13% would be expected for the DMNB group alone (Walker et al., 1993). Quantum yield cannot be calculated from our measurements, because enough of the dye was uncaged during the initial UV illumination period to significantly alter the absorbance of the solution in the cuvette.

Uncaging rate constant determination from HPTS immobilized in glycerin

A solution of 20 μM caged HPTS was mixed with 97.2% glycerin, spread as a thin film on a glass coverslip, and irradiated with a 24-μm-radius spot of 325-nm light. As described in the Methods, fluorescence of the uncaged species was excited at 458 nm, and emission was detected at wavelengths longer than 480 nm. The 325-nm radiation (132 μW on a 1.8×10^{-5} cm^2 area on the specimen) resulted in a light flux at the focal point of 7.3 W/cm^2. The uncaging reaction for caged HPTS obeyed first-order kinetics (Fig. 3 *A*) with complete photoactivation after ~15 s of illumination. The fluorescence data from four replicate measurements yielded plots linear in T_u in accordance with Eq. 9. The mean ± SD value for the uncaging reaction rate constant, K, was 0.35 ± 0.11 s^{-1}.

The rate of HPTS uncaging during pulsed illumination (0.5 mJ/5 ns) of a 3-μm-diameter spot at 355 nm was also determined. In this situation, the incident light flux at the focal point was very high, ~3×10^7 W/cm^2, and, as shown in Fig. 3 *B*, ~25% of the caged HPTS, or ~38×10^6 molecules, were released by each 5-ns light pulse.

Determination of the diffusion coefficient of uncaged dye diffusing in a thin film

When the low-molecular-weight dye HPTS was uncaged in a thin film of aqueous solution, diffusional spread from the release site was sufficiently rapid that usable quantitative information could not be obtained from the video images. Therefore, the free solution diffusion coefficient of HPTS was determined by measurement of the fluorescence intensity after uncaging, by using the multichannel PMT assembly. Fig. 4 shows a typical fluorescence decay curve when the uncaging spot was 3 μm in diameter. The mean ± SD diffusion coefficient of 17 measurements at 24°C was $D_{free} = 2.3 \pm 0.3 \times 10^{-6}$ cm^2/s, which, when corrected for 37°C, would be $3.2 \pm 0.4 \times 10^{-6}$ cm^2/s. For comparison,

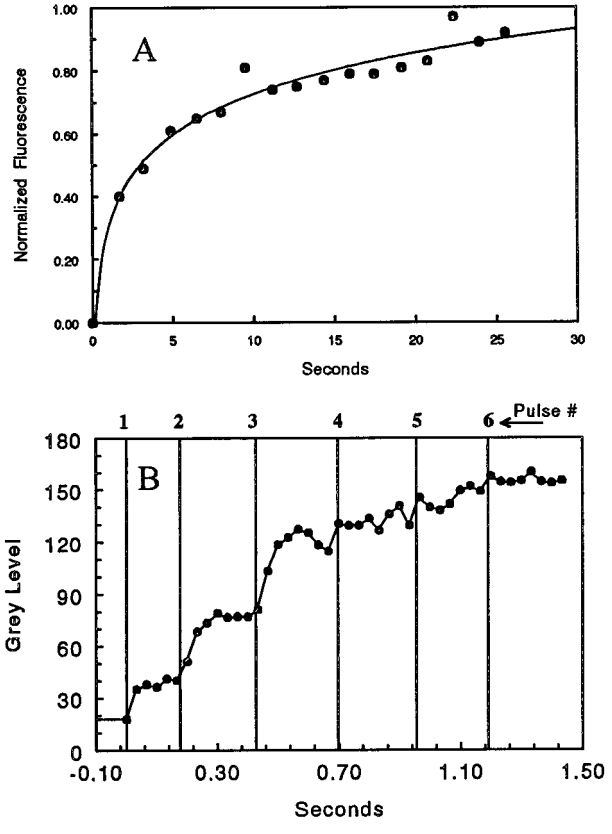

FIGURE 3 (*a*) Fluorescence intensity from a 24-μm-radius region of a thin film of caged HPTS in 97% glycerin solution after uncaging produced by 325-nm ultraviolet illumination. Fluorescence was monitored at 458 nm over the same area as that used for uncaging. The abscissa is the duration of illumination. The solid line is the best fit for an uncaging rate constant value of $K = 0.32$ s^{-1}. (*b*) Fluorescence intensity from a 3-μm spot after pulsatile illumination at 355 nm.

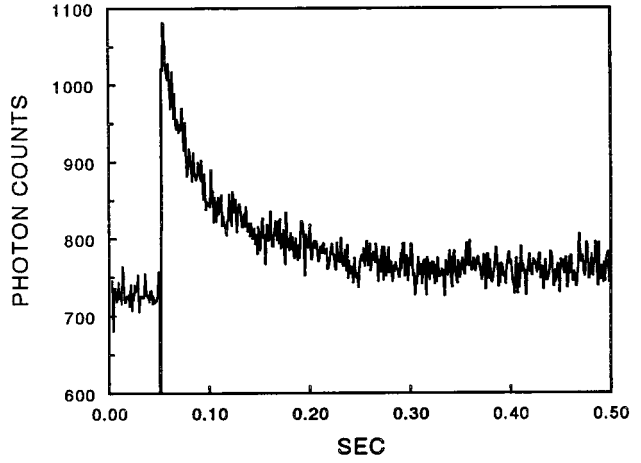

FIGURE 4 Average intensity of HPTS fluorescence from seven measurements of a 3-μm-diameter region after uncaging caused by a single pulse of 355-nm illumination. The thin film of 50 μM caged HPTS was uniformly illuminated with 458-nm light after uncaging to excite the fluorescence of the uncaged species. Fluorescence intensity, expressed as photon counts, was measured with a multichannel PMT at a sampling rate of 500 Hz.

the free solution value for sodium fluorescein (MW 332) at 37°C was reported as 7.0×10^{-6} cm^2/s (Jain, 1985).

The rate of diffusion of the 10,000 MW fluorescein dextran was considerably slower than that of HPTS, making it possible to obtain video images of the fluorescence as a function of time after uncaging. However, even with this slower molecule, the video images of the temporal decay of the fluorescence were of limited value compared with the data obtained with the multichannel PMT (Fig. 5). The mean ± SD diffusivity from the multichannel PMT data for 10,000 MW fluorescein dextran at 22°C was $D_{free} = 6.8 \pm 1.1 \times 10^{-7}$ cm^2/s ($n = 3$), corresponding to a value at 37°C of 9.8×10^{-7} cm^2/s. For comparison, experimental measurements of fluorescently labeled 10,000 MW dextran in agarose (Nicholson and Tao, 1993) yielded a mean ± SD value of $1.35 \pm 0.09 \times 10^{-6}$ cm^2/s. In addition, a value of 1.09×10^{-6} cm^2/s can be calculated from a correlation for dextrans of molecular weight between 3,000 and 200,000 Da (Preston and Comper, 1982). Recently, the diffusion coefficient of several dextrans was determined in gels by FRAP using confocal microscopy, and a value of 2.0×10^{-6} cm^2/s was obtained for 10,000 MW dextran (Cutts et al., 1995).

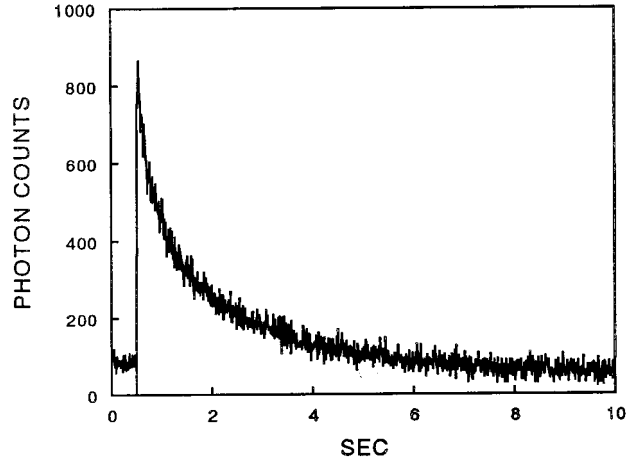

FIGURE 5 Intensity of the fluorescence of an aqueous solution of 10,000 MW caged fluorescein dextran before and after uncaging of a 50 μM solution of the caged compound. Fluorescence intensity, expressed as photon counts, was measured with the multichannel PMT at a sampling rate of 100 Hz.

Rapid uncaging within a small region of LIS

Video imaging of the time decay of fluorescence from 10,000 MW dextran uncaged within a 3-μm-diameter uncaging region of the LIS of MDCK cells grown on glass coverslips is illustrated in Fig. 6. Gray-scale values from a small region near the center of the uncaging spot in the successive video images are displayed in Fig. 7. Diffusion coefficient values were obtained from such time decay data sets; however, the covariance with the unknown initial fluorescence values was unacceptably high. As an alternative approach, the video images were analyzed for the spatial rather than the temporal variation in fluorescence. The video frame captured 0.2 s after uncaging in the experiment of Fig. 7 was used to provide the spatial intensity profile along a 10-μm length of LIS shown in Fig. 8. Because the video spatial intensity profiles were of higher quality than the temporal profiles, they were used in the regression analysis of 23 uncaging experiments to calculate values for the 10,000 MW dextran diffusion coefficient of $D_{LIS} = 2.7 \pm 0.9 \times 10^{-7}$ cm^2/s. The mean ± SD hindrance factor $\theta = 4.0 \pm 1.2$ for 10,000 MW dextran from the spatial video profiles.

When the temporal intensity profiles for the LIS uncaging region were calculated from the multichannel PMT results, the data were of higher quality than those from the concomitant video images. Fig. 9 *a* shows the PMT data from a typical experiment with the 10,000 MW dextran that yielded a diffusion coefficient $D_{LIS} = 6 \times 10^{-7}$ cm^2/s. The mean ± SD for the diffusivity in 42 experiments in the LIS of five MDCK cultures was $6.0 \pm 3.2 \times 10^{-7}$ cm^2/s, resulting in a mean ± SD hindrance factor for the 10,000 MW dextran of $\theta = 1.6 \pm 0.5$ (significantly greater than 1.0, $p < 0.01$, $n = 42$).

The relative diffusivity of HPTS in the LIS was sufficiently high that it could only be determined from the PMT data, as usable video images could not be obtained during the very brief time interval available before the diffusion diminished the dye concentration to immeasurably low levels. Fig. 9 *b* shows an example of a typical record of the PMT data for HPTS that yielded a diffusion coefficient $D_{LIS} = 3 \times 10^{-6}$ cm^2/s. The mean ± SD for the diffusion coefficient of HPTS in the LIS at 37°C was $2.8 \pm 0.6 \times 10^{-6}$ cm^2/s ($n = 14$), yielding a hindrance factor of $\theta = 1.2 \pm 0.2$, not significantly different from 1.0.

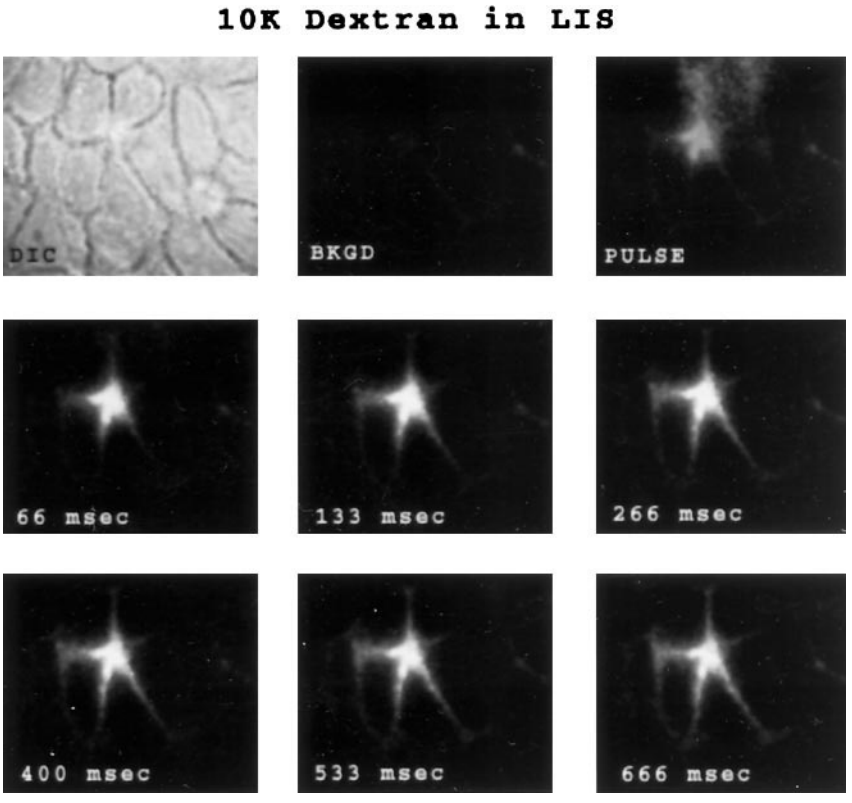

FIGURE 6 Video images of the time course of uncaging of 10,000 MW caged fluorescein dextran confined to the LIS of a MDCK monolayer. The radius of the uncaging beam was nominally 1.5 μm.

Uncaging over a monolayer region containing many cells

The large-area diffusion coefficient values for HPTS obtained from the video images of fluorescence decay after large spot uncaging with 325-nm illumination exhibited a mean $\pm$ SD value of $D_{\mathrm{LIS}} = 0.83 \pm 0.6 \times 10^{-6}$ cm^2/s (n = 8). Comparison of normalized fluorescence data with a best-fit simulation is illustrated in Fig. 10. For a geometric tortuosity factor of $\Lambda^2 = 3.1$ and a measured free solution

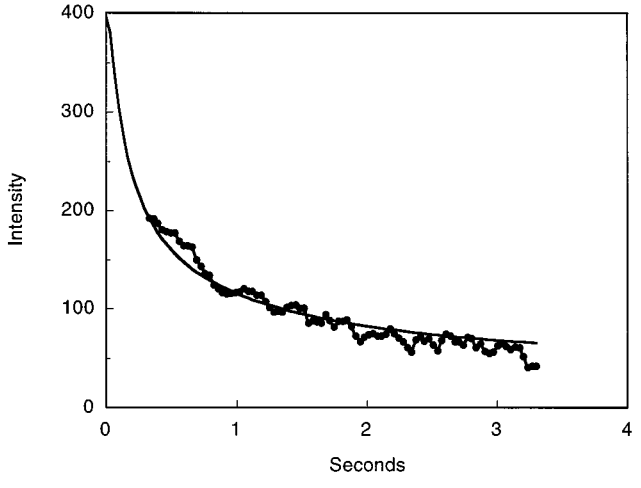

FIGURE 7 Time decay of fluorescence. The fluorescence gray-scale values, indicated by the circles, were taken from a small region near the center of the beam. The solid curve is the best-fit simulation for diffusion of the uncaged dextran with a diffusion coefficient value of 3.5×10^{-7} cm^2/s, obtained by Marquardt-Levenberg regression. In addition to D_{LIS}, the fluorescence maximum immediately after uncaging, F^{ref}, was an adjustable parameter in the regression.

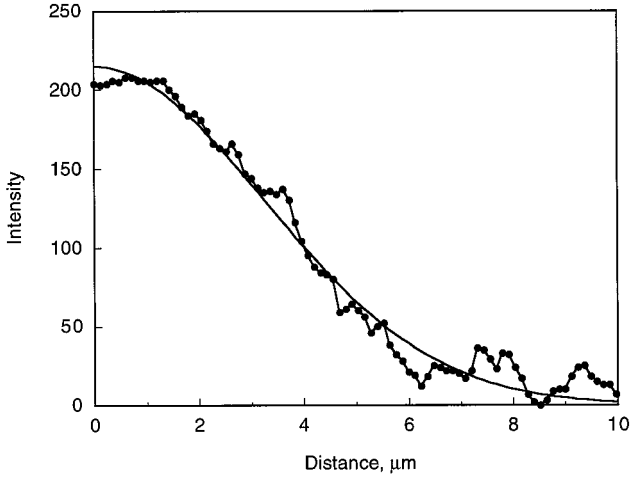

FIGURE 8 A portion of the spatial fluorescence intensity profile at 0.2 s after uncaging in the same experiment as in Fig. 7. The origin corresponds approximately to the center of the 1.5-μm radius uncaging beam. The circles represent gray-scale values of pixel-by-pixel intensity in a single video frame image (pixels were 0.115 μm in x and y). The solid line is the best-fit simulation for diffusion of the uncaged dextran with a diffusion coefficient value of 2.45×10^{-7} cm^2/s, obtained by Marquardt-Levenberg regression. A uniform background intensity of 19 was subtracted from the measured values before the regression. The background for each profile was arbitrarily chosen to be the minimum measured intensity value of that profile.

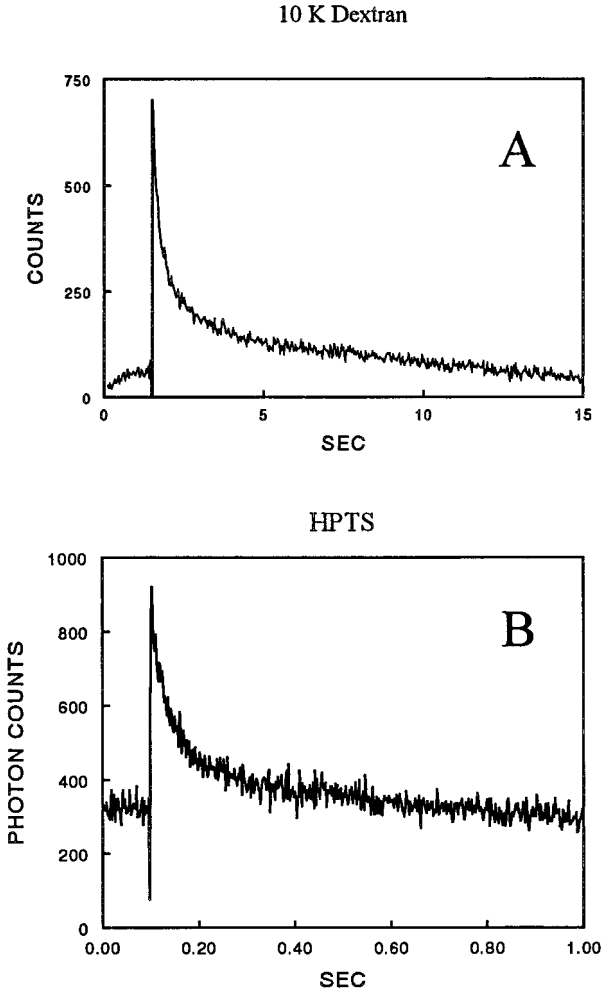

FIGURE 9 (*a*) Typical decay curve for uncaged 10,000 MW fluorescein dextran confined to the LIS of a MDCK cell monolayer, as measured with the multichannel PMT assembly. (*b*) Typical decay curve for uncaged HPTS, as measured with the multichannel PMT assembly.

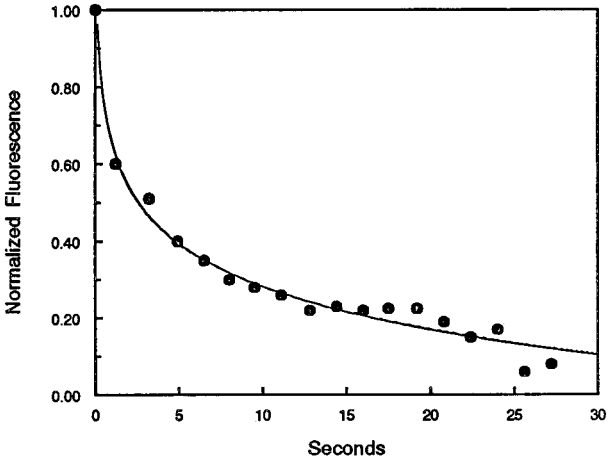

FIGURE 10 Decay of fluorescence from uncaged HPTS confined to the LIS of a MDCK monolayer after 3 s of illumination with 325-nm light. The nominal radius of the illumination region was 24 μm. The solid curve is the best-fit simulation for diffusion of caged HPTS and uncaged HPTS, yielding a hindrance factor ($\theta = 1.04$) that was assumed to be the same for both species. The free solution diffusion coefficient for caged HPTS (720 MW) was estimated from the measured value for uncaged HPTS (524 MW), assuming that the diffusion coefficients are inversely proportional to the square root of the molecular weight.

diffusivity value, D_{free}, $= 3.2 \times 10^{-6}$ cm^2/s, the hindrance factor was $\theta = D_{free}/(\Lambda^2 \cdot D_{LIS}) = 1.25 \pm 0.5$, not significantly different from 1.0.

DISCUSSION

Methodological considerations

We avoided the complexity of analyzing the diffusional spread of an uncaged fluorescent dye in three dimensions by utilizing an uncaging beam that was of uniform intensity and geometry in the axial direction. Diffusivity in free solution could then be readily analyzed as a problem in radial diffusion from a central point source. Within the LIS, we selected straight segments and only considered diffusional spread of the fluorophore in the transverse direction.

Video imaging of the uncaged fluorescent dyes allowed us to locate the uncaging beam and to analyze the spatial spread of fluorescence. Although it was possible to obtain a fit of the diffusion equation to the measured temporal decay profiles of 10,000 MW dextran within the LIS, more consistent results were obtained by using the spatial decay profiles. However, the video data always suffered from sufficient limitations in dynamic range and temporal resolution, enough to preclude measurements with small-diameter uncaging regions for small solute diffusion (e.g., HPTS) and to somewhat compromise measurements on large solutes (e.g., 10,000 MW dextran).

The temporal decay data obtained with the multichannel PMT assembly were of much higher quality than those from the video records. The high sample rate, large dynamic range, and low noise of this detector made it ideal for photoactivation experiments. Diffusion coefficients for solutes with a wide range of molecular weights could be determined with great precision and reproducibility. The full capabilities of the multichannel PMT were not employed in the present study, because the signal from only a single channel at the site of uncaging was utilized for the data analysis. Thus, comparable data could have been obtained with a single PMT equipped with a limiting iris or pinhole (Piller, 1977). However, the single-channel measurements in the present study served to meet a methodological goal—validation of the multichannel PMT approach for rapid measurements of the diffusion of small solutes. Recently we (Kovbasnjuk et al., manuscript in preparation) have utilized multiple channel recordings for the determination of the diffusivity of very rapidly diffusing species, such as ions, both in free solution and in interstitial spaces.

The combination of photoactivated fluorescence, simultaneous imaging by an intensified CCD camera, and quantitation by a multichannel PMT results in a very powerful,

versatile approach to the study of solute diffusion or convection in poorly accessible compartments in epithelia and other complex tissues. The visual cues provided by the intensified CCD camera enable the investigator to rapidly assess the quality of the uncaging and subsequent diffusion events. Acquisition and storage of the data from the entire 64-channel PMT array allow the analysis of the experiment to be carried out off-line. The high signal-to-noise and large dynamic range of the PMT detector result in very high-quality measurements compared with those obtained from the quantitation of the video images.

Diffusion coefficients in the LIS

Although the geometric tortuosity factor ($\Lambda^2 = 3.1$) takes the consequences of overall cell shape into account in the large area measurements, a further reduction in solute diffusivity within the LIS is indicated by values greater than unity obtained for the hindrance factor θ. Three factors could be result in values of θ greater than 1: subcellular tortuosity of the LIS, hindrance due to molecular structures within the LIS, or binding to charged moieties on the lateral membranes of the cells. Tortuosity of the LIS results in an underestimate of the diffusion coefficient because the path is lengthened and the assumption of linear diffusion along the LIS is incorrect. This was particularly evident in the data derived from video images of the spatial intensity profiles of the 10,000 MW dextran. The apparent value of θ was 4.0, indicative of a more substantial reduction in diffusivity than was seen with the local measurements using the PMT. The PMT measurements, derived from a more localized region in the LIS, showed that the larger solute, 10,000 MW fluorescein dextran, had a value of θ (1.6) significantly higher than 1.0 but less than 4.0. The PMT measurements also showed that diffusivity of HPTS within the LIS was similar to that in free solution and that θ was not significantly different from 1.0. Dissimilar values of θ for solutes differing by ~20-fold in molecular weight are consistent with the conclusion that the reduction in diffusivity is not the result of LIS tortuosity, but is due to molecular hindrance effects. Hindrance due to differences in charge is less likely, as both solutes are anions: HPTS has three negative charges, and the dextran exhibits one to three negative charges, depending on the labeling ratio. It is worth noting that the present measurements of diffusion coefficients in the LIS were made on MDCK epithelia grown on glass coverslips. In a previous study from our laboratory (Harris et al., 1994) utilizing FRAP and video imaging, it was reported that the diffusivity of another anionic fluorescent dye, BCECF, in the LIS of MDCK cells grown on glass was indistinguishable from that expected for the dye in free solution. Thus it seems reasonable to conclude that MDCK cells grown on glass coverslips do not substantially impede small anionic solute diffusion.

Implications for models of fluid transport

Almost all mathematical models of isosmotic fluid absorption by epithelia incorporate a restriction to ion diffusion within the LIS arising from tortuous tissue geometry and/or binding to fixed charges on the cell membranes. In these models, the balance between solute diffusion and the rate of fluid convection resulting from hydrostatic and osmotic forces is a major determinant of the osmolality of the absorbate. Most model calculations predict that rapid diffusional loss of solute from the LIS would not allow water and solute to completely equilibrate, and the absorbate would be hyperosmotic. A restricted rate of Na^+ and Cl^- diffusion within the LIS is required for the development of standing-osmotic gradients along the LIS (Diamond, 1979; Spring, 1998). Although the diffusivities of Na^+ and Cl^- within the LIS have not been measured because of technical limitations, the lack of restriction to diffusion of HPTS within the LIS observed in the present study, as well as the rapid diffusion of BCECF reported in a previous investigation (Harris et al., 1994), are not consistent with models that predict the development of intraepithelial solute gradients along the LIS during fluid absorption (Diamond and Bossert, 1967; Spring, 1998).

In summary, we have developed the theory and instrumentation to measure the rates of diffusion of a variety of photoactivatable solutes in the extracellular spaces of cultured epithelia and, presumably, in other preparations. The high speed, low noise, and wide dynamic range of the multichannel PMT detector assembly are well suited to this application. The combination of imaging by means of an intensified CCD camera and measurement by the PMT array provides complementary capabilities. Using this approach, we have shown that the small solute HPTS diffuses freely within the lateral intercellular spaces of MDCK cell epithelium, whereas the diffusivity of the larger dextran is reduced to ~60% of that in free solution.

REFERENCES

Adams, S. R., and R. Y. Tsien. 1993. Controlling cell chemistry with caged compounds. *Annu. Rev. Physiol.* 55:755–784.

Axelrod, D., D. E. Koppel, J. Schlessinger, E. Elson, and W. W. Webb. 1976. Mobility measurement by analysis of fluorescence photobleaching recovery kinetics. *Biophys. J.* 16:1055–1069.

Chatton, J. Y., and K. R. Spring. 1995. The sodium concentration of the lateral intercellular spaces of MDCK cells: a microspectrofluorimetric study. *J. Membr. Biol.* 144:11–19.

Cutts, L. S., P. A. Roberts, J. Adler, M. C. Davies, and C. D. Melia. 1995. Determination of localized diffusion coefficients in gels using confocal scanning laser microscopy. *J. Microsc.* 180:131–39.

Diamond, J. M. 1979. Osmotic water flow in leaky epithelia. *J. Membr. Biol.* 51:195–216.

Diamond, J. M., and W. H. Bossert. 1967. Standing-gradient osmotic flow. A mechanism for coupling of water and solute transport in epithelia. *J. Gen. Physiol.* 50:2061–83.

Edidin, M., Y. Zagyansky, and T. J. Lardner. 1976. Measurement of membrane protein lateral diffusion in single cells. *Science*. 191: 466–468.

Flamion, B., P. M. Bungay, C. C. Gibson, and K. R. Spring. 1991. Flow rate measurements in isolated perfused kidney tubules by fluorescence photobleaching recovery. *Biophys. J.* 60:1229–1242.

Harris, P. J., J. Y. Chatton, P. H. Tran, P. M. Bungay, and K. R. Spring. 1994. pH, morphology, and diffusion in lateral intercellular spaces of epithelial cell monolayers. *Am. J. Physiol.* 266(*Cell Physiol.* 35): C73–C80.

Jain, R. K. 1985. Transport of macromolecules in tumor microcirculation. *Biotechnol. Prog.* 1:81–94.

Kaplan, J. H., B. Forbush, III, and J. F. Hoffman. 1978. Rapid photolytic release of adenosine 5′-triphosphate from a protected analogue: utilization by the Na:K pump of human red blood cell ghosts. *Biochemistry.* 17:1929–1935.

Lempert, W. R., P. Ronney, K. R. Gee, and R. P. Haugland. 1995. Tagging velocimetry in incompressible-flow using photo-activated nonintrusive tracking of molecular-motion (PHANTOMM). *Exp. Fluids*. 18: 249–257.

Mitchison, T. J. 1989. Polewards microtubule flux in the mitotic spindle: evidence from photoactivation of fluorescence. *J. Cell Biol.* 109: 637–652.

Nicholson, C., and L. Tao. 1993. Hindered diffusion of high molecular weight compounds in brain extracellular microenvironment measured with integrative optical imaging. *Biophys. J.* 65:2277–2290.

Piller, H. 1977. Microscope Photometry. Springer-Verlag, Berlin.

Preston, B. N., and W. D. Comper. 1982. Diffusion of dextrans at intermediate concentrations. *J. Chem. Soc. Faraday Trans.* I78:1209–1221.

Smith, P. R., L. C. Stoner, S. C. Viggiano, K. J. Angelides, and D. J. Benos. 1995. Effects of vasopressin and aldosterone on the lateral mobility of epithelial Na^+ channels in A6 renal epithelial cells. *J. Membr. Biol.* 147:195–205.

Spring, K. R. 1990. Quantitative imaging at low light levels: differential interference contrast and fluorescence microscopy without significant light loss. *In* Optical Microscopy for Biology. B. Herman and K. A. Jacobson, editors. Wiley-Liss, New York. 513–522.

Spring, K. R. 1998. Routes and mechanism of fluid transport by epithelia. *Annu. Rev. Physiol.* 60:105–119.

Svoboda, K., D. W. Tank, and W. Denk. 1996. Direct measurement of coupling between dendritic spines and shafts. *Science.* 272:716–719.

Walker, J. W., H. Martin, F. R. Schmitt, and R. Barsotti. 1993. Rapid release of an α-adrenergic receptor ligand from photolabile analogues. *Biochemistry.* 32:1338–1345.

Wolfbeis, O. S., E. Fürlinger, H. Kroneis, and H. Marsoner. 1983. Fluorometric analysis. 1. A study of fluorescent indicators for measuring near neutral ("physiological") pH values. *Fresenius Z. Anal. Chem.* 314: 119–124.

Xia, P., B-E. Persson, and K. R. Spring. 1995. The chloride concentration in the lateral intercellular spaces of MDCK cell monolayers. *J. Membr. Biol.* 144:21–30.